JOURNAL OF SOLID STATE CHEMISTRY 92, 380–385 (1991)

# Valence Ordering in $V_5O_9$ Below 120 K

Y. LE PAGE,* P. BORDET,†,‡ AND M. MAREZIO†,§

*Solid State Chemistry, National Research Council of Canada, Ottawa, Canada K1AOR9 †Laboratoire de Cristallographie CNRS, associé à l'Université J. Fourier, 166X, 38042 Grenoble Cedex, France; and §AT&T Bell Laboratories, Murray Hill, New Jersey 07974*

Received November 9, 1990

The superstructure in $V_5O_9$ below 120 K is due to valence ordering and pair formation. Among the fairly large atomic displacements, one V–V distance across a shared edge between octahedra in a rutile-like chain changes from 2.860(1) Å at room temperature to 2.686(1) Å at 105 K, a distance comparable to that found in vanadium metal. The observed pairing explains the large known discontinuities in electrical conductivity and magnetic susceptibility at the 120 K transition. 

## Introduction

Many Magneli oxides display low-temperature phase transitions that are associated with abrupt changes in the electrical conductivity and magnetic susceptibility. The transition at 120 K in $V_5O_9$ (*1*) is characterized by a dramatic drop of the conductivity by about five orders of magnitude on cooling. The behavior above 120 K corresponds to semiconduction, while at lower temperatures, the logarithm of the conductivity is observed to plot linearly against temperature. This non-Arrhénius behavior is the same as that found in many other Magneli oxides (*1, 2*).

The crystal structure of this compound below 120 K is therefore of considerable interest, for elucidating the nature of both the transition and the conduction mechanism at low temperature. Following the observation of superstructures in $Ti_6O_{11}$ (*3*), $Ti_4O_7$ (*4*), $Ti_5O_9$, and $V_6O_{13}$, the unit cell of $V_5O_9$ was reexamined below the transition temperature by taking precession photographs on the same sample used in the original structural study (*5*). A superstructure corresponding to the doubling of the unit cell volume was observed (*6*). It differs from the 10-fold multiplication of cell volume observed in $Ti_5O_9$. This illustrates the individuality of each low temperature phase of these compounds, which are otherwise isostructural at room temperature.

## Experimental

The sample used for the X-ray single crystal data collection was a broken fragment of approximate size 0.25 × 0.20 × 0.15 mm from a crystal grown at NRC (*1*) by vapor transport. $TeCl_4$ was used as transport agent. The superstructure observed at 105 K was the same as that observed in (*6*). The

‡ To whom correspondence should be addressed.

0022-4596/91 $3.00

TABLE I

CRYSTAL DATA

| | 105 K | 299 K |
|---|---|---|
| $a$ | 7.0050(15) | 7.0020(20) |
| $b$ | 8.3629(15) | 8.3516(20) |
| $c$ | 10.9833(17) | 10.9052(23) |
| $\alpha$ | 91.98(2) | 91.91(2) |
| $\beta$ | 108.34(2) | 108.39(2) |
| $\gamma$ | 110.39(2) | 110.50(2) |
| Space group | $P\bar{1}$ | $B\bar{1}$ |
| Radiation | Mo$K\alpha$ | Mo$K\alpha$ |
| $2\theta$ max | 80 | 80 |
| Unique reflns | 6993 | 3482 |
| Observed ($>2.5\sigma$) | 5823 | 2824 |
| Absorpt. corr. | Gaussian | Gaussian |
| Variables | 114 (iso) | 131 (aniso) |
| $R(F)$ obs | 2.69% | 2.80% |
| $R(F)$ all | 3.51% | 3.51% |

cell parameters (Table I) were obtained by least-squares refinement of the angles of 38 accurately centered reflections with $2\theta$ Bragg angles between 70 and 80°. The diffraction intensities were measured at 105 K up to 80° $2\theta$ with graphite-monochromatized Mo$K\alpha$ radiation. The experimental conditions are otherwise identical to those in (*3*, *4*). The intensities were also measured at 299 K in the same $2\theta$ range with the same experimental technique. The shape of the crystal was approximated by 11 planar faces and a Gaussian absorption correction was applied to the intensities measured at both temperatures. The cell used here is the Buerger (or Niggli)-reduced cell, as recommended in (*7*).

## Origin Selection and Structure Solution

In the case of $Ti_4O_7$ at 140 K and $Ti_6O_{11}$ at 130 K, the origin could be selected in the middle of a segment of an octahedral rutile chain (either of type 1 or 2), because the multiplicity of the superstructure was an odd number (five and three, respectively). On the other hand, with a multiplicity of two, and assuming a centrosymmetrical structure, there are two nonequivalent possible origins, as can be shown with use of the similarity matrices: the existence of a symmetry center in the middle of such a segment excludes the existence of one at the shared edge between the segments, and vice-versa. The origin can therefore be selected on V10 in the pseudorutile region, or between two V12 atoms at the shear plane. Consequently, two MULTAN solutions corresponding to these nonequivalent origins were developed as indicated in (*3*). The atomic coordinates for the two solutions were refined concurrently, while the isotropic thermal parameters were kept fixed at $\langle U^2 \rangle = 0.003$ for the V atoms and 0.007 Å$^2$ for O. The space group was assumed to be $P\bar{1}$. The solution corresponding to the origin in the shear plane converged to 3.5%

TABLE IIa

ATOMIC PARAMETERS X, Y, Z AND Beq AT 105 K

| | $X$ | $Y$ | $Z$ | Beq |
|---|---|---|---|---|
| V10 | 0.74760(5) | 0.00644(4) | 0.75577(3) | 0.154(4) |
| V11 | 0.58784(5) | 0.78814(4) | 0.93148(3) | 0.145(4) |
| V12 | 0.43164(5) | 0.56995(4) | 0.11640(3) | 0.137(4) |
| V20 | 0.24718(5) | −0.00469(4) | 0.75262(3) | 0.166(4) |
| V21 | 0.09433(5) | 0.79979(4) | 0.91712(3) | 0.148(4) |
| V22 | 0.93607(5) | 0.57808(4) | 0.11016(3) | 0.130(4) |
| V11′ | 0.93144(5) | 0.21598(4) | 0.57272(3) | 0.145(4) |
| V12′ | 0.06263(5) | 0.42146(4) | 0.39242(3) | 0.147(4) |
| V21′ | 0.40830(5) | 0.19497(4) | 0.56580(3) | 0.133(4) |
| V22′ | 0.56156(5) | 0.40927(4) | 0.39304(3) | 0.131(4) |
| O10 | 0.48842(22) | 0.91514(16) | 0.29485(13) | 0.327(16) |
| O11 | 0.30436(21) | 0.67990(16) | 0.45289(13) | 0.311(16) |
| O20 | 0.35492(21) | 0.86954(16) | 0.87953(13) | 0.322(16) |
| O21 | 0.17669(22) | 0.63287(16) | 0.04236(13) | 0.294(16) |
| O30 | 0.20374(22) | 0.96731(16) | 0.05821(13) | 0.335(16) |
| O31 | 0.04505(22) | 0.75165(16) | 0.23477(13) | 0.347(16) |
| O32 | 0.86631(21) | 0.53543(16) | 0.40540(13) | 0.301(16) |
| O40 | 0.61988(22) | 0.79688(16) | 0.11262(13) | 0.318(16) |
| O41 | 0.47675(22) | 0.57386(16) | 0.28102(13) | 0.346(16) |
| O10′ | 0.01656(22) | 0.07691(16) | 0.20866(13) | 0.341(16) |
| O11′ | 0.19417(21) | 0.32441(16) | 0.04700(13) | 0.312(16) |
| O20′ | 0.16692(22) | 0.14495(16) | 0.62349(13) | 0.340(16) |
| O21′ | 0.32586(22) | 0.36767(16) | 0.46044(13) | 0.297(16) |
| O30′ | 0.28420(22) | 0.02054(16) | 0.43551(13) | 0.328(16) |
| O31′ | 0.45526(22) | 0.24202(16) | 0.26453(13) | 0.343(16) |
| O32′ | 0.62805(21) | 0.46083(16) | 0.09261(13) | 0.311(16) |
| O40′ | 0.87117(22) | 0.18480(16) | 0.38572(13) | 0.344(16) |
| O41′ | 0.00911(22) | 0.41016(16) | 0.21031(13) | 0.331(16) |

*Note.* e.s.ds. refer to the last digit printed. Beq is the arithmetic mean of the principal axes of the thermal ellipsoid.

TABLE IIb

ATOMIC PARAMETERS $X$, $Y$, $Z$, AND Beq AT 299 K

| | $X$ | $Y$ | $Z$ | Beq |
|---|---|---|---|---|
| V10 | $\frac{3}{4}$ | 0 | $\frac{3}{4}$ | 0.448(20) |
| V11 | 0.57992(7) | 0.79196(5) | 0.92499(4) | 0.379(14) |
| V12 | 0.43492(7) | 0.57526(5) | 0.11119(4) | 0.361(13) |
| V20 | $\frac{1}{4}$ | 0 | $\frac{3}{4}$ | 0.404(20) |
| V21 | 0.08668(7) | 0.79704(5) | 0.92329(4) | 0.399(15) |
| V22 | 0.93541(7) | 0.57951(5) | 0.10855(4) | 0.347(13) |
| O10 | 0.4864(3) | 0.92074(22) | 0.29249(17) | 0.58(6) |
| O11 | 0.3027(3) | 0.67735(21) | 0.45282(17) | 0.49(5) |
| O20 | 0.3440(3) | 0.86266(21) | 0.87832(17) | 0.53(6) |
| O21 | 0.1759(3) | 0.63329(21) | 0.04135(16) | 0.44(5) |
| O30 | 0.2119(3) | 0.97698(21) | 0.06285(16) | 0.53(6) |
| O31 | 0.0485(3) | 0.75928(21) | 0.23640(16) | 0.55(6) |
| O32 | 0.8721(3) | 0.54041(20) | 0.40543(16) | 0.47(5) |
| O40 | 0.6197(3) | 0.80036(21) | 0.10888(16) | 0.54(6) |
| O41 | 0.4820(3) | 0.58155(21) | 0.28150(17) | 0.56(6) |

*Note.* e.s.ds. refer to the last digit printed. Beq is the arithmetic mean of the principal axes of the thermal ellipsoid.

for all observed reflections, while the other did not converge. Refinement of individual isotropic thermal parameters further lowered the unweighted $R$-factor to 2.7% on 5823 observed reflections with 114 refined parameters. The $R$-factor including all 6993 independent reflections was 3.51%. The final atomic parameters are given in Table IIa.

The room temperature measurements were refined with anisotropic thermal parameters to a final $R$-factor of 2.7%, using the same cell and origin as at 105 K with space group $B\bar{1}$. The relatively poorer room temperature $R$-factor with respect to that obtained at low temperature can be explained by the considerable extinction effect on most subcell reflections. The results of this refinement are given in Tables IIb and IIc.

3467 intensity measurements taken at 95 K with graphite-monochromatized Ag$K\alpha$ radiation on the spherical sample used in (*6*) refined to $R$ = 4.6%. The positional and thermal parameters obtained in this refinement are quite close to those of Table IIa. The higher residual obtained in this case is attributed to the crude scheme for extinction correction of the SDP program used (*12*).

## Structure Description and Discussion

The present discussion of the structural aspects for the low-temperature phase supersedes that found in (*5*) because it was shown in (*6*) that the superstructure intensities, which carry the information about the valence ordering and the pair formation, had been previously overlooked. The nomenclature used here is that developed in (*8*) and used in (*9, 3, 5*) for the isostructural Ti se-

TABLE IIc

ANISOTROPIC THERMAL PARAMETERS FOR $V_5O_9$ AT 299 K

| | $U11$ | $U22$ | $U33$ | $U12$ | $U13$ | $U23$ |
|---|---|---|---|---|---|---|
| V10 | 0.560(23) | 0.598(22) | 0.604(22) | 0.304(18) | 0.187(18) | 0.097(17) |
| V11 | 0.484(17) | 0.491(16) | 0.529(15) | 0.218(13) | 0.222(13) | 0.133(12) |
| V12 | 0.461(15) | 0.473(15) | 0.462(15) | 0.226(12) | 0.141(12) | 0.049(11) |
| V20 | 0.517(23) | 0.539(22) | 0.605(22) | 0.259(18) | 0.279(18) | 0.230(17) |
| V21 | 0.514(17) | 0.484(16) | 0.656(16) | 0.249(13) | 0.285(13) | 0.256(12) |
| V22 | 0.417(15) | 0.478(15) | 0.431(15) | 0.149(12) | 0.183(12) | 0.080(11) |
| O10 | 0.73(7) | 0.85(6) | 0.81(7) | 0.41(5) | 0.38(5) | 0.31(5) |
| O11 | 0.56(6) | 0.65(6) | 0.69(6) | 0.25(5) | 0.22(5) | 0.20(5) |
| O20 | 0.64(6) | 0.77(6) | 0.80(6) | 0.38(5) | 0.36(5) | 0.31(5) |
| O21 | 0.49(6) | 0.66(6) | 0.60(6) | 0.29(5) | 0.21(5) | 0.20(5) |
| O30 | 0.76(7) | 0.60(6) | 0.61(6) | 0.20(5) | 0.27(5) | 0.07(5) |
| O31 | 0.80(7) | 0.68(6) | 0.65(6) | 0.29(5) | 0.29(5) | 0.12(5) |
| O32 | 0.63(6) | 0.56(6) | 0.67(6) | 0.25(5) | 0.28(5) | 0.12(5) |
| O40 | 0.78(7) | 0.67(6) | 0.58(6) | 0.23(5) | 0.26(5) | 0.13(5) |
| O41 | 0.76(7) | 0.74(6) | 0.64(6) | 0.28(5) | 0.23(5) | 0.18(5) |

TABLE III

AVERAGE V–O DISTANCES FOR $VO_6$ OCTAHEDRA AND FORMAL VALENCES OF V ATOMS

| | 105 K | | 299 K | |
|---|---|---|---|---|
| | ⟨V–O⟩ (Å) | Valence (v.u.) | ⟨V–O⟩ (Å) | Valence (v.u.) |
| V12′ | 2.002 | 3.180 | | |
| V11′ | 1.993 | 3.230 | | |
| V10 | 1.976 | 3.359 | 1.956 | 3.549 |
| V11 | 1.996 | 3.180 | 1.974 | 3.420 |
| V12 | 1.967 | 3.799 | 1.970 | 3.657 |
| V22′ | 1.957 | 3.859 | | |
| V21′ | 1.964 | 3.821 | | |
| V20 | 1.934 | 3.860 | 1.948 | 3.640 |
| V21 | 1.953 | 3.783 | 1.966 | 3.562 |
| V22 | 1.953 | 3.875 | 1.966 | 3.623 |

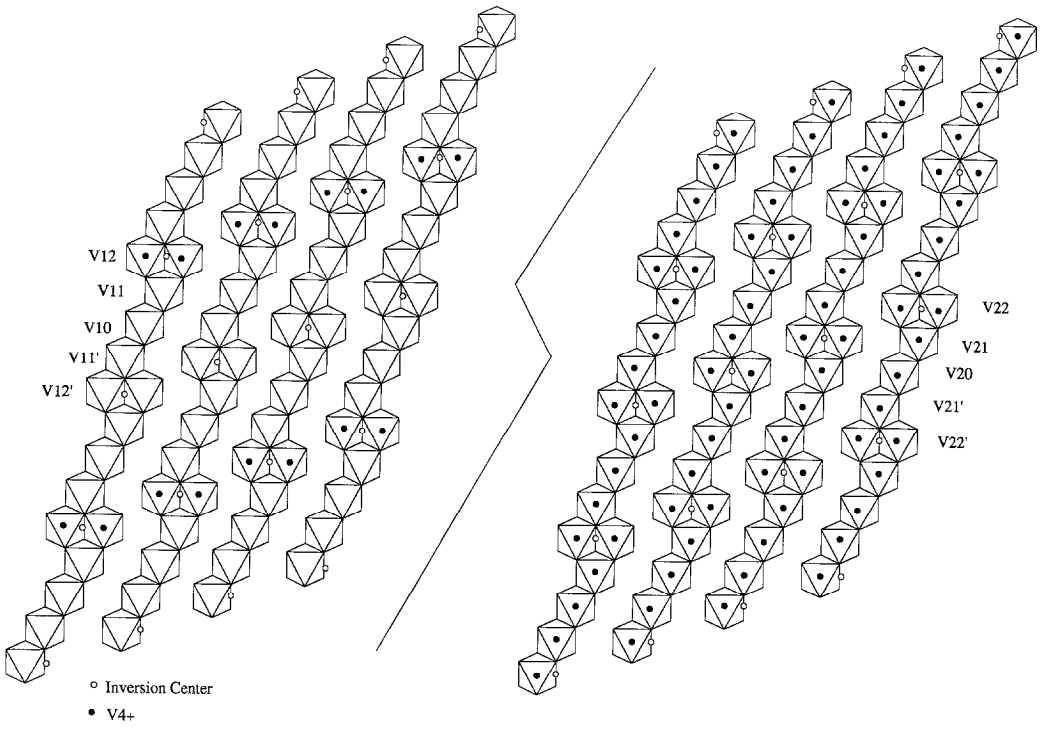


FIG. 1. Schematic representation of the low-temperature phase structure of $V_5O_9$ showing two adjacent octahedral layers parallel to the pseudo-*hcp* layers of oxygen atoms. The distribution of the $V^{4+}$ cations (full circles) is shown.

ries. The two indices following the atom type indicate, respectively, the chain type and the sequence number in the chain, counted from the center of the rutile block. The correspondence of the atom names with those of Andersson and Jahnberg (*10*) used in (*5*) is given in Table IV of (*8*) for the isostructural compound $Ti_5O_9$. Due to the absence of a symmetry center in V10 and V20, the low-temperature motif comprises a complete chain segment of each type extending from one shear plane to the next. It follows that the two atoms with the same second index in the same segment are now inequivalent and are distinguished with a single quote. There are now two kinds of shear planes: those which comprise V12 and V22 and those which comprise V12′ and V22′.

The valences of the V atoms were analyzed as indicated in (*3, 4*). The individual room-temperature valences (Table III) differ little from the stoichiometric average 3.6 valence units (v.u.) that can be derived from the chemical formula. On the other hand, at low temperature, the observed valences split into two classes: four V atoms carry about 3.2 v.u. while the remaining six carry approximately 3.85 v.u. This strongly indicates that the charges are localized in the low-temperature phase. The departure from the ideal values of 3+ and 4+, respectively, may be attributed to domain formation and/or to incomplete localization due to the fact that 105 K is too close to the transition temperature.

Figure 1 shows the two octahedral layers parallel to the pseudohexagonal close-packed planes of oxygen atoms. In the low temperature phase, the layers correspond to

the V1*n* and V2*n* atoms, respectively, each layer containing the shared edges between the pseudorutile segments at the symmetry center. The V2*n* layer is exclusively made of $V^{3.85+}$ ions, while the V1*n* layer is made of $V^{3.2+}$ ions with the exception of the V12 ion, which is 3.8+. This situation is reminiscent of the case of $Ti_4O_7$ below 120 K (*13, 4*) and $V_4O_7$ below 250 K (*14*), where *hcp* layers are alternately 3+ and 4+. However, in the present case, the stoichiometry requires two $V^{3+}$ ions for every three $V^{4+}$ ones, but a similar two-layer scheme seems to occur.

The known sharp discontinuity in the electrical conductivity and in the magnetic susceptibility at the 120 K transition (*1, 2*) can be interpreted in light of the present structural results (Fig. 2, Tables III and IV),

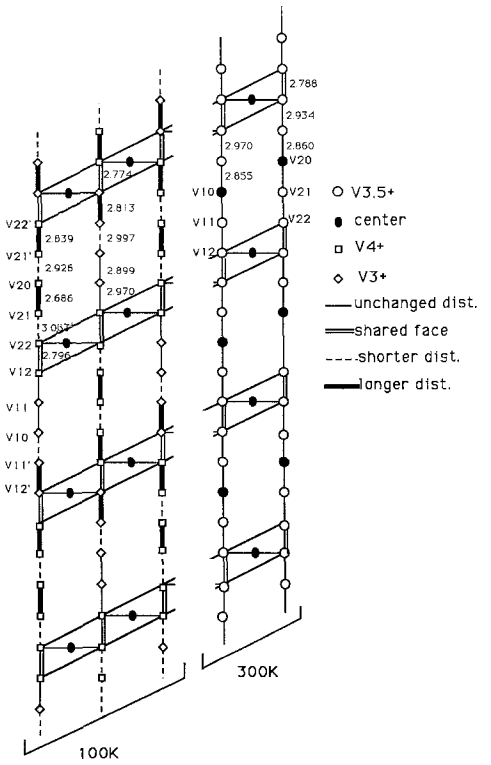


FIG. 2. Schematic representation of the changes in metal–metal distances between room temperature and 100 K in $V_5O_9$.

TABLE IV

V–V DISTANCES IN THE CHAIN

| 299 K | | | | 105 K | |
|---|---|---|---|---|---|
| V10–V11 | 2.855 | V10–V11 | 2.899 | V10–V11′ | 2.997 + + |
| V11–V12 | 2.970 | V11–V12 | 2.971 | V11′–V12′ | 2.813 − − − |
| V12–V22 | 2.788 | V12–V22 | 2.796 f | V12′–V22′ | 2.773 f |
| V22–V21 | 2.934 | V22–V21 | 3.063 + + | V22′–V21′ | 2.839 − − |
| V21–V20 | 2.860 | V21–V20 | 2.686 − − − | V20–V21′ | 2.926 + |

*Note.* The shared faces are indicated by f. The + and − signs indicate bonds that lengthened or shortened respectively by more than 0.05 Å on cooling. The interchain distances do not display any remarkable changes. The e.s.ds on distances are 0.01 Å.

which support pair formation at low temperature between V21′–V22′ and V20–V21 along the rutile chains. The valences of these atoms become 4+ and the metal–metal distances decrease by more than 0.15 Å. The V20–V21 distance becomes 2.686 Å, which is shorter than the distance in $VO_2$ (about 2.85 Å). Pair formation is also observed at V11′–V12′ in the rutile chains where the distance decreases by 0.15 Å while the valences of both vanadium cations decrease. On the other hand, pair formation does not occur at V12–V22 and V12′–V22′ at the shared faces between the segments, since the distance does not decrease while the average valence of the vanadium cations increases (for V12–V22) or is the same (for V12′–V22′) in the low-temperature phase. This leaves only the electrons on the atoms V10, V11, V12, and V22 available for conduction and magnetic susceptibility, the remaining part of the structure having become essentially insulating and nonmagnetic. The magnetic moments remaining on these atoms are probably responsible for the known magnetic transition occurring at 30 K (*15*). A neutron diffraction experiment would elucidate the magnetic structure of this interesting compound.

## References

1. A. D. INGLIS, C. M. HURD, AND P. STROBEL, *J. Phys. C* (1984).
2. A. D. INGLIS, Y. LE PAGE, P. STROBEL, AND C. M. HURD, *J. Phys. C: Solid State Phys.* **16,** 317 (1983).

3. Y. LE PAGE AND P. STROBEL, *J. Solid State Chem.* **47,** 6 (1983).
4. Y. LE PAGE AND M. MAREZIO, *Solid State Chem.* **53,** 13 (1984).
5. M. MAREZIO, P. D. DERNIER, D. B. MCWHAN, J. P. REMEIKA, AND S. KACHI, *J. Solid State Chem.* **11,** 301 (1974).
6. P. BORDET, J. J. CAPPONI, AND M. MAREZIO, *C.R. Acad. Sci. Paris, Série II* **296,** 1775 (1983).
7. *Acta Crystallogr.,* Notes for Authors.
8. Y. LE PAGE AND P. STROBEL, *J. Solid State Chem.* **43,** 314 (1982).
9. Y. LE PAGE AND P. STROBEL, *J. Solid State Chem.* **44,** 273 (1982).
10. S. ANDERSSON AND L. JAHNBERG, *Ark. Kem.* **21,** 413 (1963).
11. H. HORIUCHI, M. TOKONAMI, N. MORIMOTO, K. NAGASAWA, Y. BANDO, AND T. TAKADA, *Mater. Res. Bull.* **6,** 833 (1971).
12. SDP: Structure Determination Package. Enraf-Nonius Delft, Holland.
13. C. SCHLENKER AND M. MAREZIO, *Philos. Mag. B* **42,** 453 (1980).
14. M. MAREZIO, D. B. MCWHAN, P. D. DERNIER, AND J. P. REMEIKA, *J. Solid State Chem.* **6,** 419 (1973).
15. S. KACHI, K. KOSUGE, AND H. OKINAKA, *J. Solid State Chem.* **6,** 258 (1973).